Available online at www.sciencedirect.com
ScienceDirect
Journal of Solid State Chemistry 181 (2008) 1240–1248
JOURNAL OF SOLID STATE CHEMISTRY
www.elsevier.com/locate/jssc

Pressure induced phase transformation in $U_2O(PO_4)_2$

A.K. Mishra[a,*], Chitra Murli[a], A. Singhal[b], Surinder M. Sharma[a]

[a]*High Pressure Physics Division, Bhabha Atomic Research Centre, Mumbai 400085, India*
[b]*Chemistry Division, Bhabha Atomic Research Centre, Mumbai 400085, India*

Received 14 November 2007; received in revised form 7 February 2008; accepted 13 February 2008
Available online 4 March 2008

Abstract

The high pressure behavior of $U_2O(PO_4)_2$ has been investigated with the help of Raman scattering and X-ray diffraction measurements up to ~14 and 6.5 GPa, respectively. The observed changes in the Raman spectra as well as the X-ray diffraction patterns suggest that $U_2O(PO_4)_2$ undergoes a phase transition at ~6 GPa to a mixture of a disordered ambient pressure phase and a new high pressure phase. The new phase resembles the triclinic mixed-valence phase of uranium orthophosphate ($U(UO_2)(PO_4)_2$). On release of pressure the initial phase is not retrieved.

Keywords: $U_2O(PO_4)_2$; Phase transition; Raman scattering; X-ray diffraction

1. Introduction

Diuranium oxide phosphate belongs to a family of tetravalent metal oxide phosphates which are represented by $M_2O(PO_4)_2$ (where $M = U$, Zr, Th, etc.). These compounds are used as thermal-shock resistant ceramics, composites and are also considered as potential candidates for the long-term storage of nuclear waste due to their low solubility in water [1,2]. These materials are also of interest in areas of ion exchange [3,4] and protonic conduction [5,6]. Due to the open framework structure, these compounds can also provide some zeolitic features, such as accessible open spaces, rigid frameworks, chemical/thermal stability, size, and shape selectivity and catalytically active sites [7,8]. In particular, diuranium oxide phosphate, iso-structural to $Zr_2O(PO_4)_2$ (an ultra-low thermal expansion ceramic), shows a continuous thermal contraction [9].

At ambient conditions, $U_2O(PO_4)_2$ exists in orthorhombic structure with space group *Cmca* (space group no. 64) [10]. In this structure, distorted UO_7 pentagonal bi-pyramids share an O(1)–O(1) edge with three equivalent PO_4 tetrahedra as shown in Figs. 1a and b. These pentagonal bi-pyramids are tightly connected as pairs in the (100) plane by strong U–O(3)–U bridging, forming infinite zigzag chains along [100] by sharing O(1)–O(1) edges. The PO_4 tetrahedra also share corners with UO_7 polyhedra. Earlier studies on sintered rods have shown that $U_2O(PO_4)_2$ has macroscopic negative thermal expansion (NTE) in the 20–1000 °C range [9]. However, subsequent studies showed that it has anisotropic thermal expansion behavior, positive thermal expansion in [100] and [001] directions and NTE in [010] direction [11]. Recent neutron and X-ray diffraction studies have shown that its NTE behavior results mainly from a polyhedra—rocking mechanism, somewhat similar to what is now believed to be the cause of NTE in monodentate framework structures such as α-ZrP_2O_7 [12] and ZrW_2O_8 [13].

In recent years, the behavior of several compounds having NTE property has been investigated under pressure. These include $Al_2(WO_4)_3$ [14], $Sc_2(WO_4)_3$ [15], $Y_2(WO_4)_3$ [16], $Zr(WO_4)_2$, and $Hf(WO_4)_2$ [17–19], etc. These studies suggest that for these compounds K' (pressure derivative of bulk modulus) may be either negative or very small [20]. Moreover, many of these compounds show various intermediate structural transformations before eventual amorphization at high pressures. In general, many of the transformations in the materials having framework structures are brought about by the ease of bending across the

*Corresponding author. Fax: +91 22 25505151.
E-mail address: akmishra@barc.gov.in (A.K. Mishra).

0022-4596/$ - see front matter © 2008 Elsevier Inc. All rights reserved.
doi:10.1016/j.jssc.2008.02.020

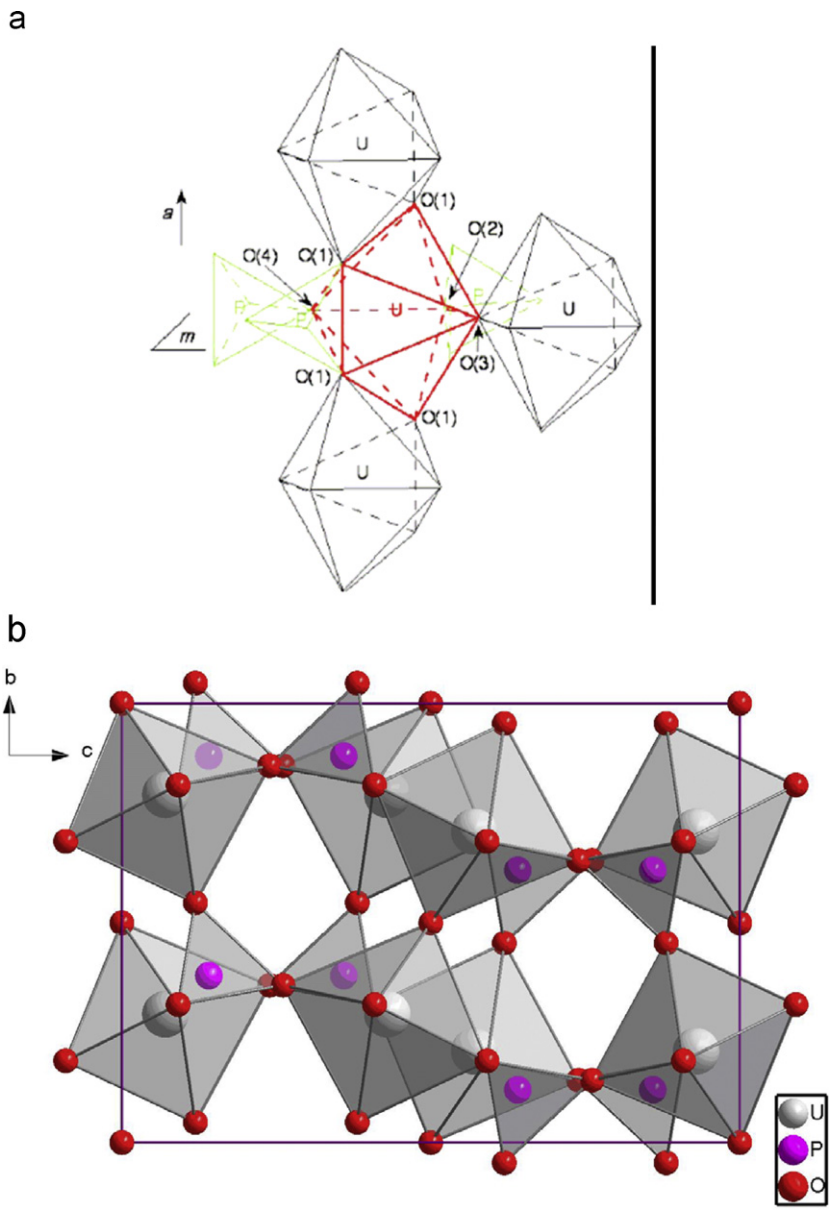

Fig. 1. (a) Edge shared UO_7 (pentagonal bipyramids) and PO_4 (tetrahedra) as in $U_2O(PO_4)_2$ and (b) the parent orthorhombic structure as viewed along [100].

polyhedral linkages aided by different compressibilities of the constituent polyhedra. These facilitate the emergence of higher coordinated structures, such as observed in α-SiO_2 (quartz), α-$AlPO_4$, α-$GaPO_4$, α-GeO_2, etc. [21–24]. Amongst these, the compounds having PO_4 tetrahedra are found to show interesting structural changes. For example, in α-$AlPO_4$, AlO_4 tetrahedra are more easily transformed to octahedrally coordinated AlO_6 resulting in the transformation to orthorhombic *Cmcm* phase at ~12 GPa. In contrast, the more rigid PO_4 retains its tretrahedral coordination to quite high pressures, i.e. upto ~70 GPa. [23,24].

As $U_2O(PO_4)_2$ comprises of UO_7 polyhedra and PO_4 tetrahedra, it would be interesting to investigate the evolution of its structure under pressure. With this in view we have carried out high pressure Raman and X-ray diffraction studies on this compound up to 14 and 6.5 GPa, respectively.

2. Experimental details

2.1. Synthesis

The diuranium oxide phosphate was synthesized using wet chemical route, as described in Ref. [10]. For this, uranium metal is dissolved in 6 M HCl to make a concentrated solution of tetravalent uranium. This solution is then mixed with concentrated phosphoric acid (5 M H_3PO_4), at room temperature. This mixture is evaporated and annealed under argon flow. Annealing under argon

environment prohibits the oxidation of $U_2O(PO_4)_2$ and consequent formation of triclinic $U^{IV}(U^{VI}O_2)(PO_4)_2$, which otherwise takes place in air at $\geqslant 300\,^{\circ}C$ [25]. The unit cell parameters of $U_2O(PO_4)_2$, determined through X-ray diffraction measurements, were found to be, $a = 7.052 \pm 0.003$ Å, $b = 8.991 \pm 0.004$ Å, and $c = 12.673 \pm 0.004$ Å. These values compare well with the cell parameters published earlier viz., $a = 7.087$ Å, $b = 9.036$ Å, $c = 12.702$ Å [11].

2.2. Experimental

The powdered sample of $U_2O(PO_4)_2$ was loaded in a hole of ~130 μm diameter of a tungsten gasket which was pre-indented to a thickness of 80 μm in a Mao–Bell type of diamond anvil cell [26]. Raman scattering experiments have been carried out under quasi-hydrostatic as well as non-hydrostatic pressures. For quasi-hydrostatic measurements, 4:1 methanol–ethanol mixture was used as a pressure transmitting medium, which is known to remain hydrostatic up to ~10 GPa [27] and quasi-hydrostatic beyond due to the soft nature of solidified alcohol mixture. In the Raman scattering experiments ruby R-lines were

Table 1
Correlation diagram of internal vibrations of $U_2O(PO_4)_2$ based on:

	C_s (site group)	D_{2h} (factor group)
(*a*) *PO_4 site symmetry group*		
T_d (molecular group)		
E(R) (360 cm^{-1})	A (IR, R)	A_g, B_{1g}, B_{2u}, B_{3u}
F_2^1 (IR, R) (500 cm^{-1})	A″(IR, R)	A_u, B_{2g}, B_{3g}, B_{1u}
A1 (R) (970 cm^{-1})		
$F_2^{(2)}$ (IR, R) (1080 cm^{-1})		
(*b*) *UO_7 site symmetry group*		
D_{5h} (molecular group)		
A_1', A_2', E_1', E_2'	A (IR, R)	A_g, B_{1g}, B_{2u}, B_{3u}
A_1'', A_2'', E_1'', E_2''	A″ (IR, R)	A_u, B_{2g}, B_{3g}, B_{1u}

The known frequencies of the isolated $(PO_4)^{3-}$ tetrahedron are given in the parenthesis [38].

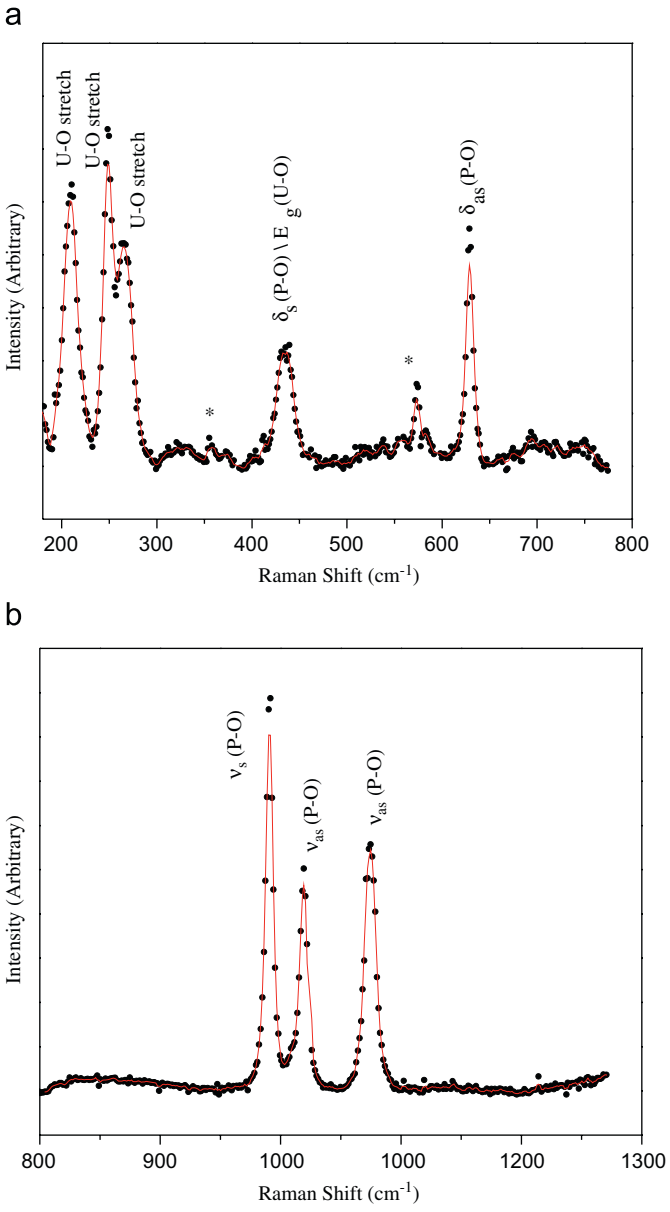

Fig. 2. Raman spectrum of $U_2O(PO_4)_2$ at ambient conditions in the spectral region: (a) 180–800 cm^{-1}, (b) 800–1300 cm^{-1}, * indicates unidentified peaks.

Table 2
Tentative assignment of observed Raman modes of diuranium oxide phosphate

Frequencies (cm^{-1})	Tentative assignments [30]
207	External modes and/or U–O stretch mode
247, 266	U–O stretch modes
433	δ_s(P–O) (symmetric bending mode) and/or E_g U–O stretch
629	δ_{as}(P–O) (asymmetric bending mode) and/or 207 + 433 = 640 (overtone of U–O stretch)
881	Unassigned
1002	ν_s(P–O)
1030, 1087	ν_{as}(P–O)

used for the pressure calibration [28], whereas for the X-ray diffraction experiments platinum was used as a pressure marker. In the latter case, the pressure on the sample was deduced using the equation of state of platinum [29].

For Raman measurements, we have used our indigenous micro-Raman system with confocal optics. The Raman scattered light from the sample, which is excited by 532 nm laser line of the diode-pumped solid state laser, is collected using a CCD based single stage spectrograph and a super-notch filter. The Raman modes in the spectral range 180–1200 cm^{-1} have been recorded as a function of pressure up to 14 GPa. Neon (Ne) and Mercury (Hg) lines were used for calibration purpose.

Angle dispersive X-ray diffraction measurements have been carried out using Mo ($K\alpha$) monochromatized X-rays ($\lambda = 0.71069$ Å) from a Rigaku rotating anode X-ray generator. The X-rays are collimated to ~100 μm and the two-dimensional diffraction rings, collected on a MAR345 imaging plate, are converted to one-dimensional diffraction profiles using the FIT2D software [30]. The cell parameters were determined using Le Bail analysis as incorporated in the GSAS software [31]. The diffraction pattern was recorded up to ~7 GPa and on release of pressure.

3. Results and discussion

3.1. Raman modes under ambient conditions

As mentioned above, at ambient conditions, $U_2O(PO_4)_2$ has orthorhombic structure (space group *Cmca* (space group no. 64), point group *mmm* (D_{2h}), four formula units per unit cell). Its factor group is isomorphous to the point group D_{2h}, and its order $g = 8$. As the conventional unit cell is **C** face centered, a primitive unit cell having two formula units can be chosen which would have 26 atoms. Thus, $U_2O(PO_4)_2$ has 75 fundamental vibrational modes, which can be classified in terms of irreducible representations as follows:

$$\Gamma_{U_2O(PO_4)_2} = 11A_g + 7B_{1g} + 7B_{2g} + 11B_{3g} + 8A_u + 12B_{1u} + 12B_{2u} + 7B_{3u}.$$

The polyhedral molecules $(PO_4)^{3-}$ and UO_7 occupy the site symmetry C_s (C_{1h}). One of the oxygen occupies site symmetry C_{2h} and another occupies C_1. The correlation diagrams, given in Table 1a and b show factor group splitting of various modes of PO_4 and UO_7 in the orthorhombic system of $U_2O(PO_4)_2$.

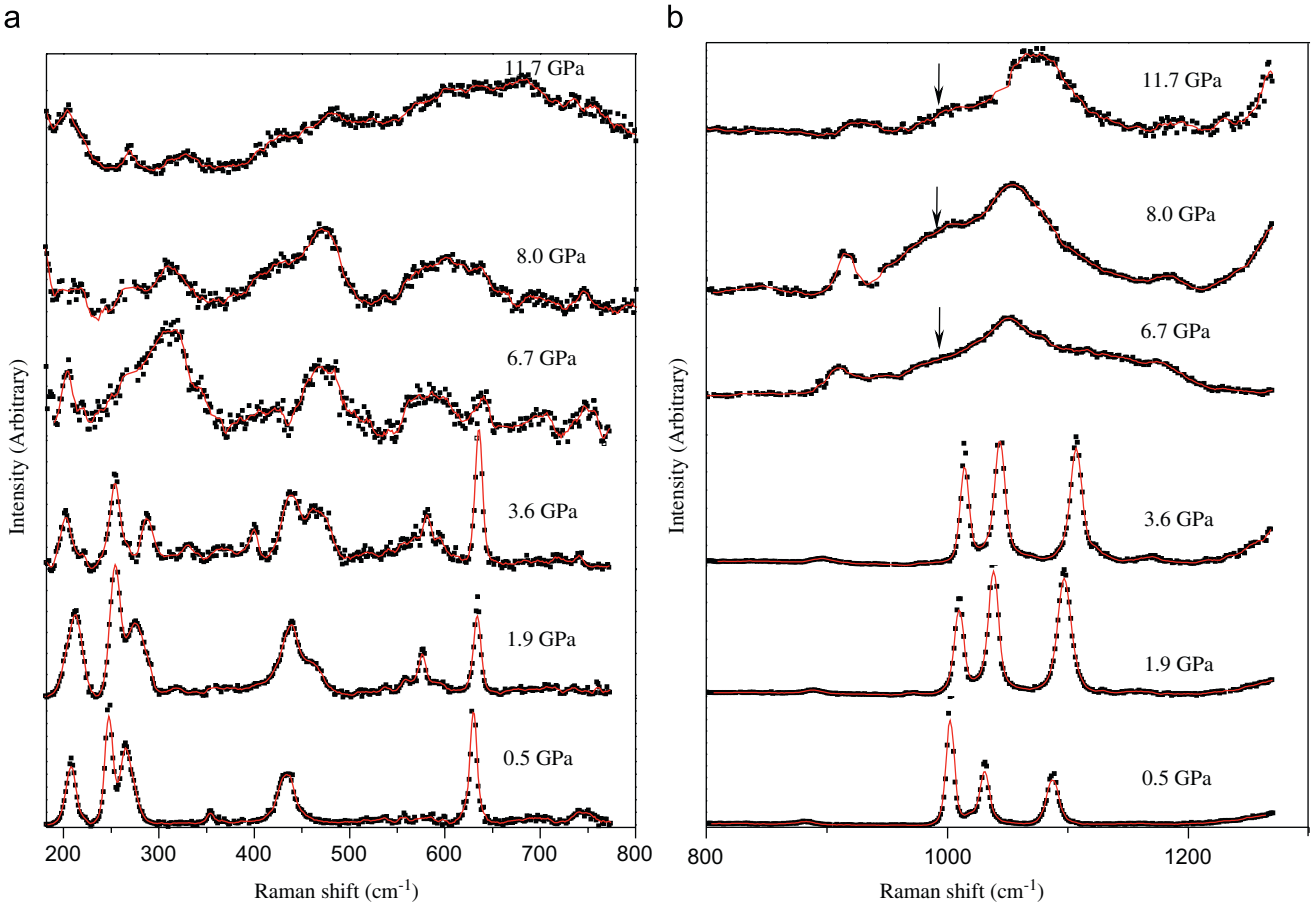

Fig. 3. Raman spectra of $U_2O(PO_4)_2$ under hydrostatic conditions in the spectral region: (a) 180–800 cm^{-1} and (b) 800–1300 cm^{-1}. Arrows indicate the emergence of a red-shifted band.

Fig. 2 shows the observed Raman spectrum of this compound in the spectral region 180–1200 cm^{-1}. As no lattice dynamical calculations are available in the literature for this compound, we adapt the mode assignments from the infrared and Raman studies on various structural modifications of uranium phosphate [32,33]. Thus, the assignments for the observed Raman modes, given in Table 2, should be viewed as tentative.

3.2. High pressure Raman studies

The Raman modes of $U_2O(PO_4)_2$, recorded in the spectral region 180–1200 cm^{-1}, and under quasi-hydrostatic and non-hydrostatic pressures are shown in Figs. 3 and 4, respectively. (The solid line running through all the Raman spectra has been obtained through 5 point averaging and should be taken as a guide to the eye.) And corresponding pressure induced changes in the positions of Raman modes are shown in Figs. 5 and 6, respectively.

In the case of hydrostatic pressures, all the observed modes were found to display gradual stiffening with pressure up to 2 GPa. The Raman mode at 207 cm^{-1} (U–O stretch) shows broadening at very low pressures (~2 GPa), while the modes at 247 and 266 cm^{-1} (U–O stretch) show significant broadening at somewhat higher pressure (~3.6 GPa). The band observed at 433 cm^{-1} shows splitting beyond 2 GPa. As this band is tentatively assigned to δ_s(P–O) and E_g(U–O) stretch modes, it is possible that these modes separate out at higher pressures. At the same pressure, the PO_4 asymmetric stretch mode at 1030 cm^{-1} (ν_{as}(P–O)) shows increase in the relative intensity with respect to the mode at 1002 cm^{-1} (ν_s(P–O)). The relative intensity of the U–O stretch mode observed at 207 cm^{-1} with respect to PO_4 stretching modes reduces significantly at pressures above 6 GPa. We also find that beyond 6.7 GPa, various Raman modes of the initial structure are replaced by broad bands in the region 300–700 cm^{-1} and the intense mode δ_{as}(P–O) observed at 629 cm^{-1} under ambient conditions becomes almost unobservable beyond this pressure. The vanishing of intensity of this mode beyond 6.7 GPa is found to be rather abrupt. At the same pressure, the Raman mode observed at 881 cm^{-1} ((ν_s(P–O)) is found to pick up intensity. Above 7 GPa, the sharper peaks corresponding to PO_4 modes are replaced by a broad band around the asymmetric stretching mode. All the features mentioned above suggest that the structure becomes increasing disordered as the pressure is increased.

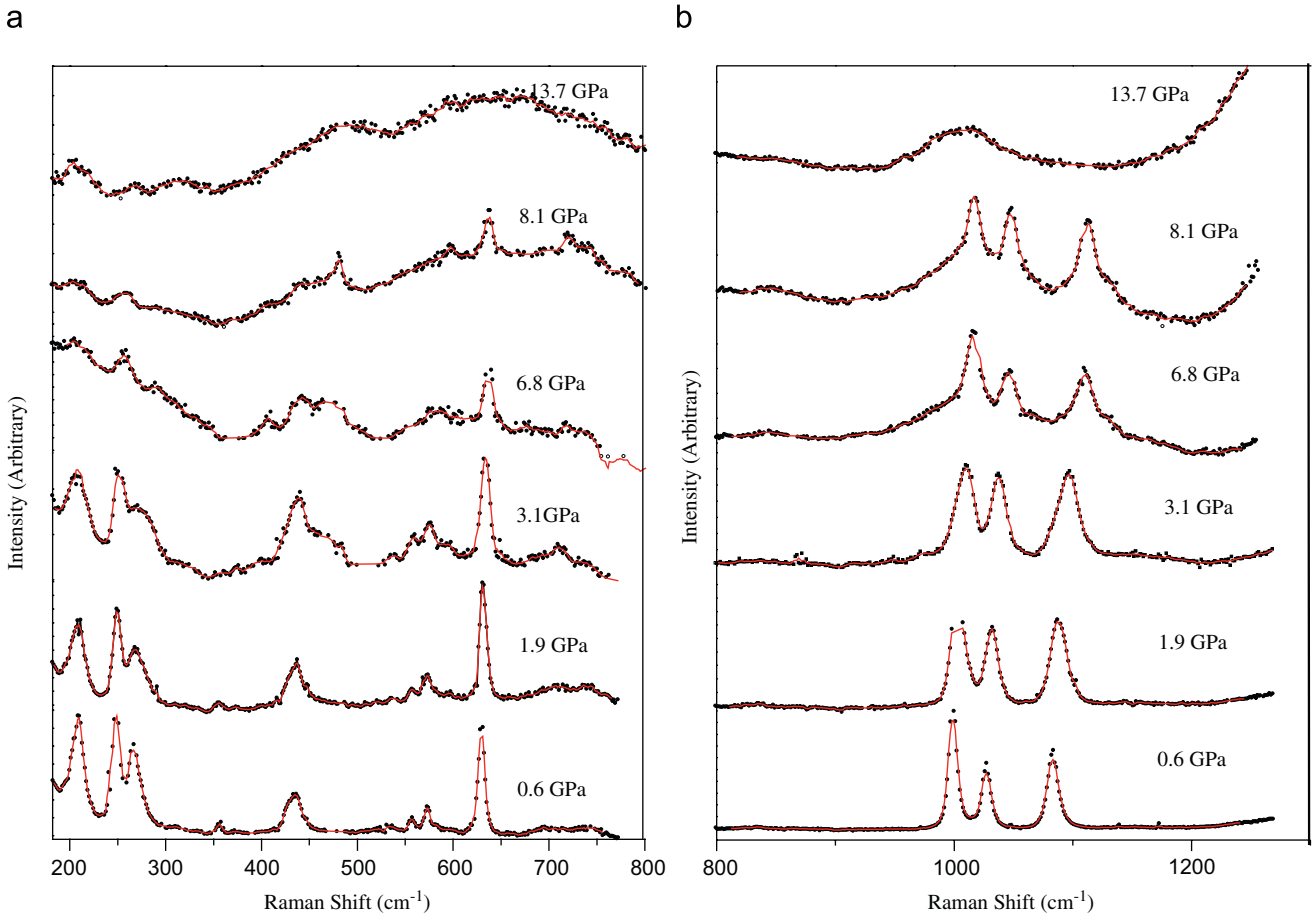

Fig. 4. Raman spectra of $U_2O(PO_4)_2$ under non-hydrostatic conditions in the spectral region: (a) 180–800 cm^{-1} and (b) 800–1300 cm^{-1}.

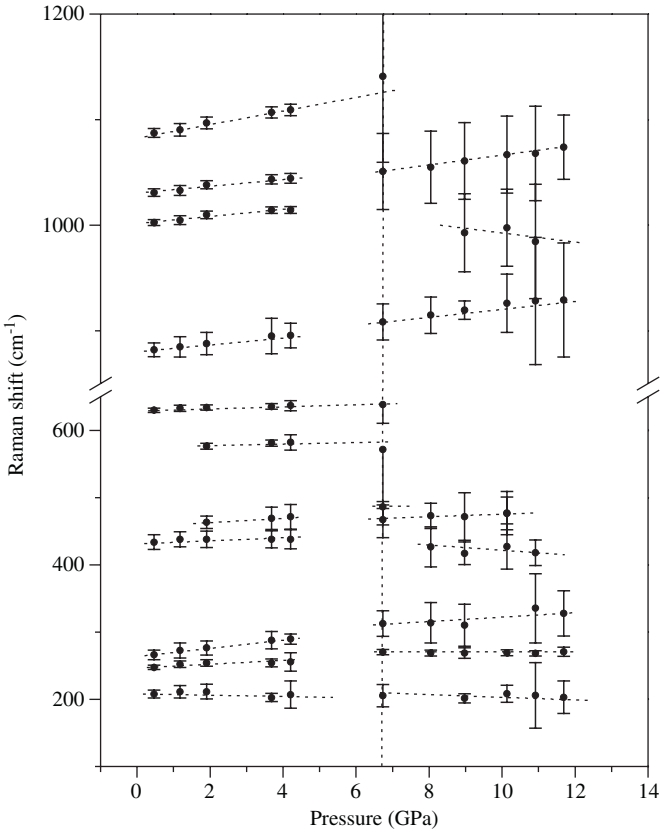

Fig. 5. Variation of Raman mode frequencies with pressure under hydrostatic conditions. (Error bars are larger beyond 6 GPa due to broad Raman peaks.)

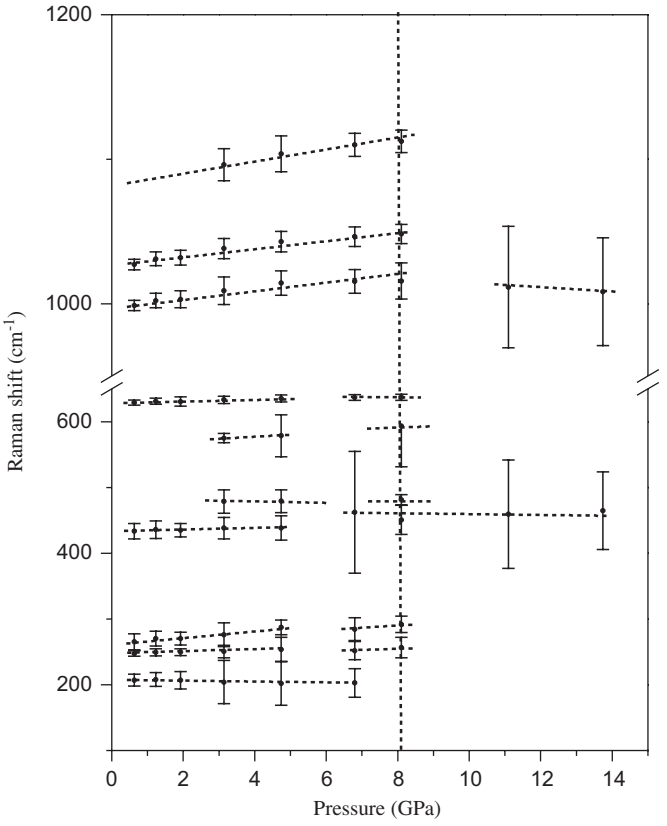

Fig. 6. Variation of Raman mode frequencies with respect to pressure under non-hydrostatic conditions.

Unlike under hydrostatic pressures, the results under non-hydrostatic conditions do not display any significant intensity redistribution amongst the internal PO_4 modes. In addition, we found that the modes at 1002 cm^{-1} (ν_s(P–O)), 1030 and 1087 cm^{-1} (ν_{as}(P–O)), continue to exist up to ~8 GPa and beyond this pressure all these modes merged into a single broad band. We note that this broad band is also red-shifted compared to the centroid of earlier peaks. We should also point out that this feature is somewhat different from the results under hydrostatic pressures, where we observed two bands, i.e. one corresponding to the centroid of the evolving peaks and another one that is red-shifted with respect to these (marked with arrow in Fig. 3b). The emergence of these red-shifted broad bands is similar to what has also been reported earlier for $Sc_2(WO_4)_3$ [15] where these were ascribed to the emergence of higher coordinated disordered state. In general, as in the hydrostatic case, the observed pressure induced broadening of the Raman modes of PO_4 as well as UO_7 polyhedra suggest that $U_2O(PO_4)_2$ becomes progressively more disordered at higher pressures.

To summarize, the overall evolution of the Raman modes and existence of a structural transition are common to both hydrostatic and non-hydrostatic conditions. However, the transition pressure for the non-hydrostatic conditions (~8 GPa) is slightly higher than that for the hydrostatic pressures (~6 GPa). Due to the fact that non-hydrostatic pressures in a DAC also imply heterogeneous stress distribution, one generally observes broadening of the peaks at lower pressures. In this sense the loss of sharp Raman features at a higher pressure under non-hydrostatic conditions is counter-intuitive and hence interesting which may encourage further work. We may speculate that such a difference for the two different stress conditions could be because the anisotropic stresses delay the partial transformation to the mixed valence phase.

As shown in Fig. 7, Raman spectra on release of pressure are similar for hydrostatic as well as non-hydrostatic conditions. An interesting feature in these spectra is the emergence of a new mode at ~870 cm^{-1} and when the retrieved sample from the hydrostatic experiments was coincidentally investigated after one month, it showed that 870 cm^{-1} mode gains intensity and in addition the broad band at ~1000 cm^{-1} is replaced by some of the sharper modes. This observed Raman spectrum closely resembles the spectrum of the $U(UO_2)(PO_4)_2$, a mixed-valence phase of uranium orthophosphate [34].

Earlier investigations on many NTE materials have attempted to interpret the observed NTE using mode Grüneisen parameters [18]. There has been varied opinions about the contribution of various energy modes to NTE and in earlier studies mostly the low energy modes

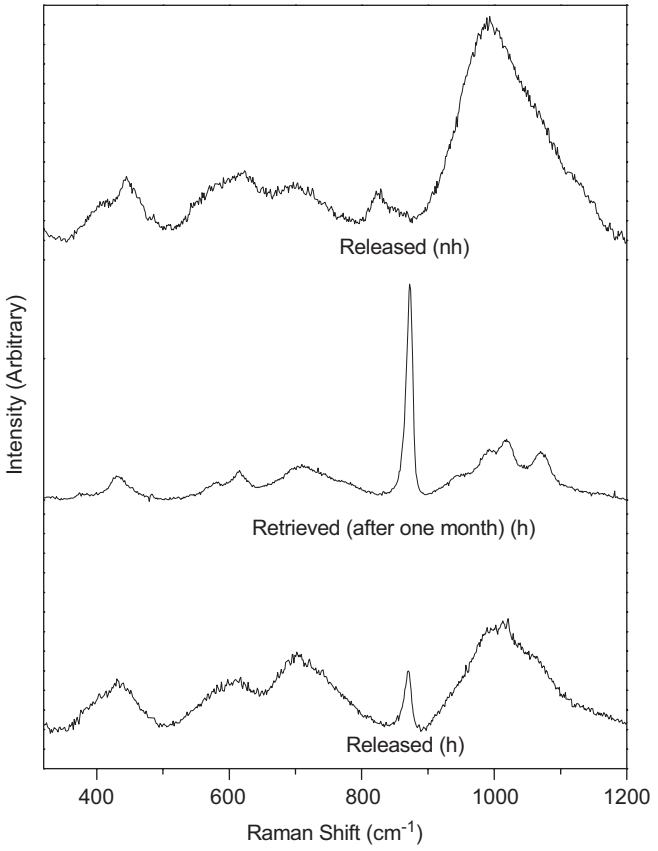

Fig. 7. Raman spectra of the $U_2O(PO_4)_2$ on release of pressure (h) denotes from hydrostatic and (nh) denotes from non-hydrostatic conditions.

Table 3
Raman mode frequencies (ν_i), their pressure dependence ($d\nu_i/dP$) and corresponding Grüneisen parameters (γ_i) in the orthorhombic *Cmca* phase of $U_2O(PO_4)_2$

ν_i (cm^{-1})	$d\nu_i/dP$ ($cm^{-1}\,GPa^{-1}$)	γ_i
207	−1.37	−0.41
247	1.65	0.41
266	1.15	0.26
433	0.71	0.10
629	1.54	0.15
881	3.79	0.26
1002	3.29	0.20
1030	3.71	0.22
1087	5.99	0.34

($\leqslant$10 meV) have been shown to be of relevance [17,35] ($d\nu/dP$) and the corresponding mode Grüneisen parameters for $U_2O(PO_4)_2$ are given in Table 3. Among the observed modes, the Raman mode at 207 cm^{-1} (~25 meV), which is tentatively assigned to U–O stretching mode, shows negative Grüneisen parameter. It is also of interest to note that in the high temperature study of $U_2O(PO_4)_2$ one of the U–O bonds was found to show NTE coefficient [11]. To gain more insight into the importance of various modes (particularly the rigid unit modes, RUMs) in affecting the observed results and NTE, it would be useful to carry out lattice dynamical calculations on this compound.

3.3. X-ray diffraction studies

Fig. 8 shows the X-ray diffraction profiles of $U_2O(PO_4)_2$ at a few representative pressures. The observed variations of the *d*-spacing with pressure are given in Fig. 9. The diffraction peaks of the pressure marker (platinum) and gasket (tungsten) are marked as *Pt*(*hkl*) and *W*(*hkl*), respectively. Our data show (Fig. 8) that with the increase of pressure many of the diffraction peaks of the ambient phase lose intensity and by ~5.5 GPa the diffraction pattern becomes quite weak and has broad features. On further increase of pressure, the diffraction peaks of $U_2O(PO_4)_2$ broadened substantially, while the diffraction peaks from the pressure marker and the gasket continue to be sharp. Across 5.5 GPa, we also observe discontinuous changes in the *d*-spacings of the diffraction peaks indicating the possibility of a structural phase transition at this pressure.

In the diffraction pattern at ~6 GPa, we find that the remnant diffraction peaks lie close to the known diffraction peaks of the lower symmetry triclinic phase of mixed valence uranium orthophosphate $U(UO_2)(PO_4)_2$.

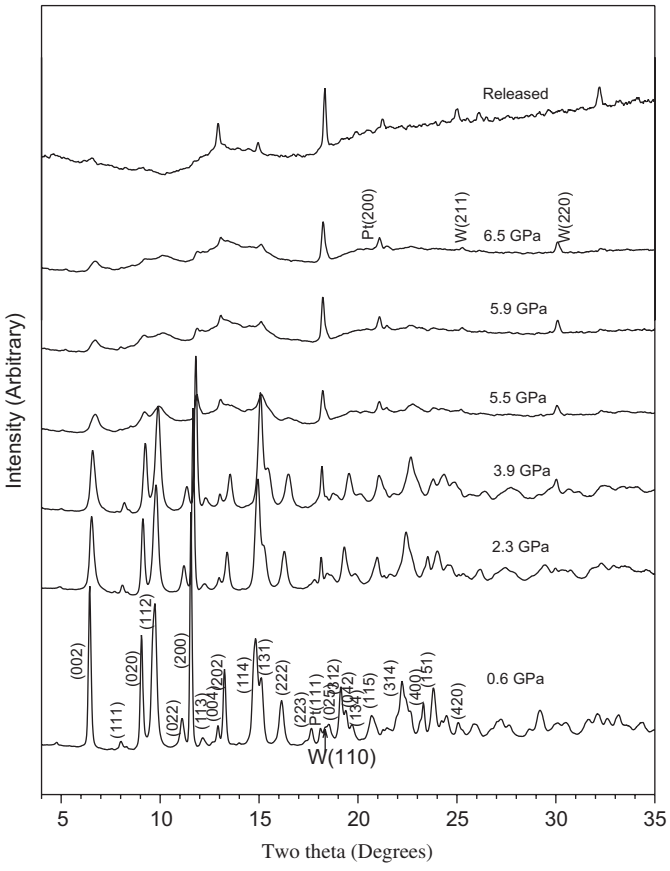

Fig. 8. X-ray diffraction patterns of $U_2O(PO_4)_2$ at a few representative pressures.

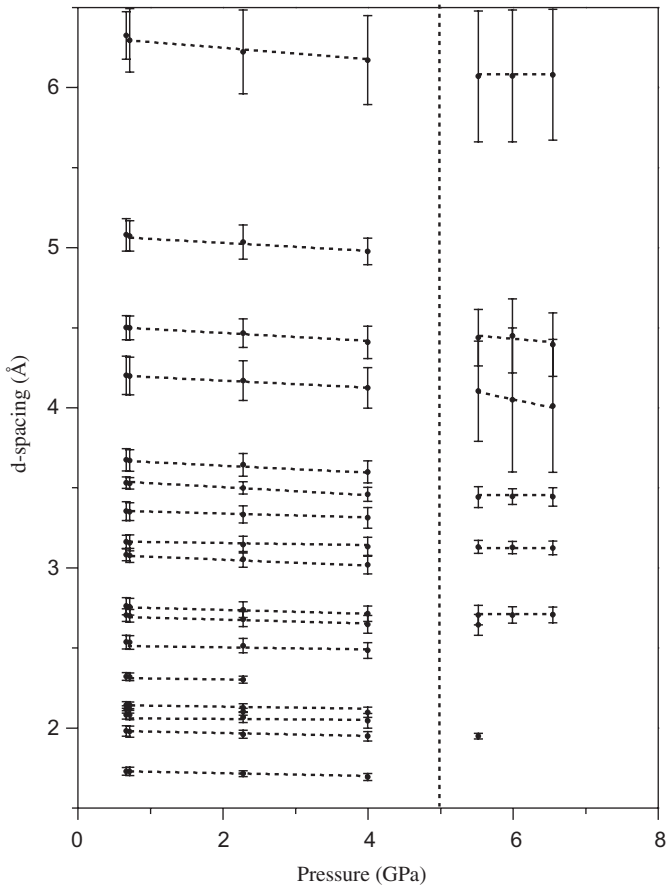

Fig. 9. Variation of d_{hkl} with pressure.

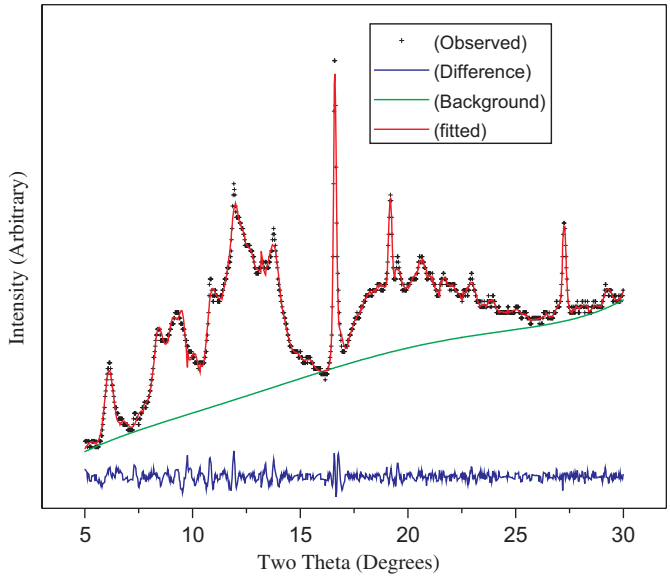

Fig. 10. Le Bail fit to the diffraction pattern at 6 GPa, both the parent orthorhombic and high pressure triclinic phases have been fitted.

Consistent with our Raman results, Le Bail fit to the diffraction data at ~6 GPa (Fig. 10) indicates it to be a mixture of initial orthorhombic and a new triclinic phase the cell parameters of which were $a = 8.795 \pm 0.003$ Å, $b = 9.302 \pm 0.002$ Å, $c = 5.483 \pm 0.002$ Å, $\alpha = 102.81° \pm 0.0003°$, $\beta = 97.00° \pm 0.0004°$, $\gamma = 102.04° \pm 0.0005°$. These values are reasonably close to the earlier reported cell parameters of the mixed valence phase, i.e. $a = 8.8212$ Å, $b = 9.2173$ Å, $c = 5.4772$ Å, $\alpha = 102.622°$, $\beta = 97.748°$, $\gamma = 102.459°$ [34]. However, the quality of the diffraction data beyond ~6 GPa is not favorable for the Rietveld analysis and hence more detailed information about the structure of the daughter phase cannot be deduced. For the parent phase, our P–V data (up to ~6 GPa) when fitted to Birch–Murnaghan equation of state [36] gives the bulk modulus and its derivative to be $\sim 61 \pm 8$ GPa and $\sim 1.4 \pm 3.1$, respectively (see Fig. 11).

Both the Raman as well as X-ray diffraction data suggest that the abundance of the disordered parent phase increases with the increase of pressure. In fact the data also points out that the new phase, similar to the one of the mixed valence of uranium, is also poorly crystallized. These results suggest the transformation to the daughter phase is kinetically frustrated giving rise to the increasing abundance of disorder [37]. In view of the fact that this compound partially transforms to the more stable crystalline phase at high pressures, we do not identify the high pressure phase as the pressure induced amorphous phase and instead term it as poorly crystallized state. These results also suggest that it would be useful to carry high pressure, high temperature X-ray diffraction experiments to obtain more information about the details and the mechanism of the pressure induced transformation in this compound.

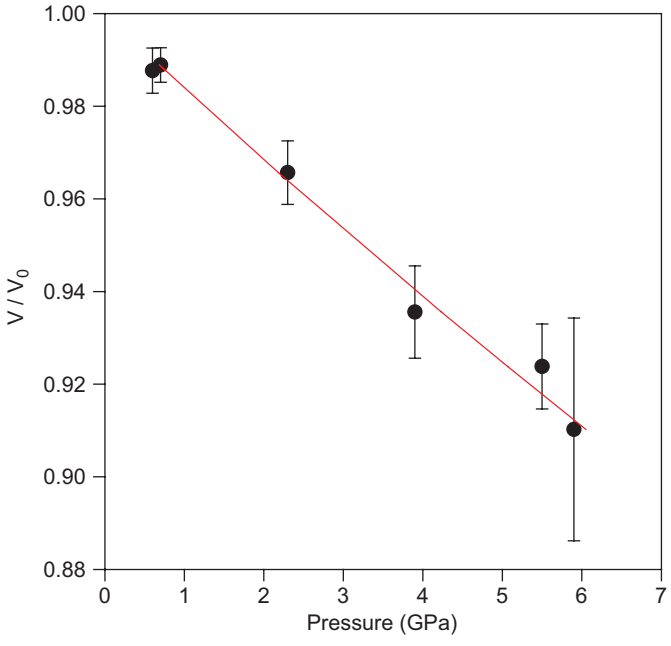

Fig. 11. V/V_0 versus pressure for the orthorhombic phase. The solid line is fit to Birch–Murnaghan equation of state [36].

4. Conclusion

Our in situ high pressure Raman and X-ray diffraction studies on the $U_2O(PO_4)_2$ show that this material undergoes a pressure induced structural transition at ~6 GPa to a mixture of disordered parent and poorly crystallized new triclinic phase. The new phase is quite similar to that of the mixed valence uranium orthophosphate. Our Raman data also suggests that the parent phase is not retrieved on release of pressure and instead the abundance of the triclinic phase increases.

References

[1] W. Schreyer, J.F. Schairer, J. Petrol. 2 (1961) 324.
[2] B.A. Bender, T.L. Jessen, S. Browning, Ceram. Eng. Sci. Prod. 16 (1995) 613.
[3] M.M. Olken, R.N. Biagioni, A.B. Ellis, Inorg. Chem. 22 (1983) 2128.
[4] M. Pham Thi, P. Colombai, J. Less-Common Met. 108 (1985) 189.
[5] B. Morosin, Acta Crystallogr. Sect. B 34 (1978) 3732.
[6] B. Morosin, Phys. Lett. A 65 (1978) 53.
[7] G.J. Hutchins, C.S. Heneghan, I.D. Hudson, S.H. Taylor, Nature 384 (1996) 341.
[8] S.H. Taylor, R. O'leary, Appl. Catal. B 25 (2000) 137.
[9] H.P. Kirchner, K.M. Merz, W.R. Brown, J. Am. Ceram. Soc. 46 (1963) 137.
[10] P. Benard, D. Louer, N. Dacheux, V. Brandel, M. Genet, An. Quim. 92 (1996) 79.
[11] G. Wallez, S. Launay, M. Quarton, N. Dacheux, J.-L. Soubeyroux, J. Solid State Chem. 177 (2004) 3575.
[12] N. Khosrovani, V. Korthnis, A.W. Sleight, Inorg. Chem. 35 (1996) 485.
[13] T.A. Mary, J.S.O. Evans, T. Vogt, A.W. Sleight, Science 272 (1996) 90.
[14] N. Garg, V. Panchal, A.K. Tyagi, S. M Sharma, J. Solid State Chem. 178 (2005) 998.
[15] N. Garg, C. Murli, A.K. Tyagi, S.M. Sharma, Phys. Rev. B 72 (2005) 1.
[16] S. Karmakar, S.K. Deb, A.K. Tyagi, S.M. Sharma, J. Solid State Chem. 177 (2004) 4087.
[17] T.R. Ravindran, A.K. Arora, T.A. Mary, Phys. Rev. Lett. 84 (2000) 3879.
[18] T.R. Ravindran, A.K. Arora, T.A. Mary, J. Phys. Condens. Matter 13 (2001) 11573.
[19] B. Chen, D.V.S. Muthu, Z.X. Liu, et al., Phys. Rev. B 64 (2001) 214111.
[20] S.K. Sikka, J. Phys. Condens. Matter 16 (2004) S1033.
[21] C. Murli, S.M. Sharma, S.K. Kulshreshtha, S.K. Sikka Pramana, J. Phys. 49 (1997) 285.
[22] S.M. Sharma, N. Garg, S.K. Sikka, Phys. Rev. B. 62 (2000) 8824.
[23] N. Garg, S.M. Sharma, J. Phys. Condens. Matter 12 (2000) 375–397.
[24] J.P. Porres, A.M. Saitta, A. Polian, J.P. Itie, M. Hanfland, Nat. Mater. 6 (2007) 698.
[25] V. Brandel, N. Dacheux, M. Genet, R. Podor, J. Solid State Chem. 159 (2001) 139.
[26] H.K. Mao, P.M. Bell, Carnegie Institute of Washington Year Book, 1978.
[27] G.J. Piermarini, et al., J. Appl. Phys. 44 (1973) 5377.
[28] H.K. Mao, J. Xu, P.M. Bell, J. Geophys. Res. 91 (1986) 4673.
[29] A. Dewaele, P. Loubeyre, M. Mezouar, Phys. Rev. B 70 (2004) 094112.
[30] A.P. Hamersley, S.O. Svensson, M. Hanfland, A.N. Fitch, D. Hausermann, High Pressure Res. 14 (1996) 235.
[31] A.C. Larson, R.B. Von Dreele, GSAS: General Structure Analysis System, Los Alamos National Laboratory, 2000.
[32] V. Brandel, N. Clavier, N. Dacheux, J. Solid State Chem. 178 (2005) 1054.
[33] S.D. Senanayake, R. Roussean, D. Colegrave, H. Idriss, J. Nucl. Mat. 342 (2005) 179.
[34] P. Benard, D. Louer, N. Dacheux, V. Brandel, M. Genet, Chem. Mater. 6 (1994) 1049.
[35] A.L. Goodwin, C.J. Kepert, Phys. Rev. B 71 (2005) 140301.
[36] F. Birch, J. Geophys. Res. 57 (1952) 227.
[37] S.M. Sharma, S.K. Sikka, Prog. Mater. Sci. 40 (1996) 1.
[38] L. Börnstein, Physikalisch-chemische Tabellen, vol. 2, Teil, 1951.